Earth and Planetary Science Letters 491 (2018) 226–237

Contents lists available at ScienceDirect

Earth and Planetary Science Letters

www.elsevier.com/locate/epsl

Magmatic controls on axial relief and faulting at mid-ocean ridges

Zhonglan Liu [a,b,*], W. Roger Buck [b]

[a] Key Laboratory of Orogenic Belts and Crustal Evolution, School of Earth and Space Sciences, Peking University, Beijing 100871, China
[b] Lamont–Doherty Earth Observatory of Columbia University, Palisades 10964, NY, USA

ARTICLE INFO

Article history:
Received 9 August 2017
Received in revised form 20 March 2018
Accepted 23 March 2018
Available online xxxx
Editor: R. Bendick

Keywords:
mid-ocean ridges
magmatism
axial relief
faulting
dike intrusion

ABSTRACT

Previous models do not simultaneously reproduce the observed range of axial relief and fault patterns at plate spreading centers. We suggest that this failure is due to the approximation that magmatic dikes open continuously rather than in discrete events. During short – lived events, dikes open not only in the strong axial lithosphere but also some distance into the underlying weaker asthenosphere. Axial valley relief affects the partitioning of magma between the lithosphere and asthenosphere during diking events. The deeper the valley, the more magma goes into lithospheric dikes in each event and so the greater the average opening rate of those dikes. The long-term rate of lithospheric dike opening controls faulting rate and axial depth. The feedback between axial valley depth D and lithospheric dike opening rate allows us to analytically relate steady-state values of D to lithospheric thickness H_L and crustal thickness H_C. A two-dimensional model numerical model with a fixed axial lithospheric structure illustrates the analytic model implications for axial faulting. The predictions of this new model are broadly consistent with global and segment-scale trends of axial depth and fault patterns with H_L and H_C.

1. Introduction

Mid-ocean ridges are the main places where magma exits the Earth's interior and new oceanic lithosphere is created and faulted. Thus, understanding the processes responsible for major spreading center features should give insight into the solid and fluid mechanics affecting other geologic systems such as continental rifts. The across-axis topographic shape of ridges show systematic variations with spreading rate (Macdonald, 1982; Small, 1998). Fast spreading centers (plate separation rates >8 cm/yr) are characterized by up axial high with up to 500-m of relief, while slow spreading ridges (plate separation rates <4 cm/yr) feature valleys as deep as 2 km (Fig. 1). Extensional faults exist at all ridges but there is a general increase in fault offset with decreasing spreading rate (Cannat et al., 2006; Carbotte and Macdonald, 1994; Small, 1998; Tucholke et al., 1998). The fault patterns show several different modes (Cannat et al., 2006; Carbotte and Macdonald, 1994) with a clear relation between magma input and fault mode (Buck et al., 2005; Tucholke et al., 2008).

In this paper we first describe previous spreading center models that fail to explain both axial relief and faulting pattern observations. We argue that to explain these observations requires consideration of the discrete nature of short-lived (i.e. hours to days) dike opening events at the axis of spreading. To do this, we need to parameterize the effect of individual dike events in a way that enables estimation of the effect of many such events on the long-term development of spreading center relief and faulting patterns. We build on previous studies of dike opening (Pollard, 1976; Qin and Buck, 2008; Weertman, 1971) to derive analytic relations between axial lithospheric thickness, the driving stress opening a dike and the distance of penetration of a dike into the asthenosphere. This analysis shows that the deeper the axial valley, the less magma goes into dikes opening into the asthenosphere. The magma intruded into the asthenosphere cools slowly to form gabbro and is not available to accommodate lithospheric plate separation.

Averaging over many dike events, we calculate the long-term flux of magma into the lithospheric part of dikes. We show that this lithospheric dike flux increases with axial depth, suggesting a way that magma supply could directly control axial depth. As long as the lithospheric dike opens at less than the plate spreading rate, then fault slip deepens the axial valley. If the valley gets deep enough that the dikes open as fast as the plates spread, then the valley stops deepening.

Numerical simulations of plate spreading are developed using these new analytic dike-opening relations to show that magma supply can control axial relief and affect near-ridge faulting. Assuming dikes supply all the magma to build the oceanic crust, we

* Corresponding author at: Key Laboratory of Orogenic Belts and Crustal Evolution, School of Earth and Space Sciences, Peking University, Beijing 100871, China.
E-mail address: zlliu-sess@pku.edu.cn (Z. Liu).

https://doi.org/10.1016/j.epsl.2018.03.045
0012-821X/

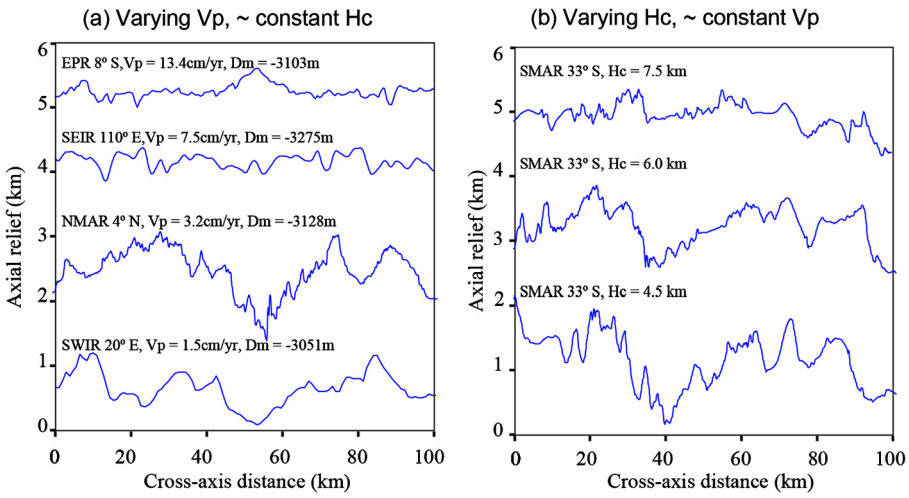

Fig. 1. Bathymetric profiles showing axial relief for different values of (a) spreading rate and (b) crustal thickness. V_P is full spreading rate; H_C, crustal thickness; Dm is mean depth within 40 km of the spreading axis defined by Small (1998) and should depend primarily on crustal thickness. EPR is the East Pacific Rise; SEIR, Southeast Indian Ridge; NMAR, Northern Mid-Atlantic Ridge; SWIR, Southwest Indian Ridge; SMAR, Southern Mid-Atlantic Ridge. Data from multibeam bathymetry are available at http://www.geomapapp.org/. Crustal thicknesses for different cross-sections of the 33°S segment of the SMAR are based on Tolstoy et al. (1993).

analytically describe how steady-state axial depth depends on axial lithospheric thickness and crustal thickness. Finally, we discuss how axial valley relief can be maintained by flexural stresses in the lithosphere when magma controls the axial valley depth and faulting does not accommodate plate spreading.

2. Previous models for spreading center relief and faulting

Global compilations show that axial relief depends on both spreading rate and crustal thickness (Small, 1998) (also see Fig. 1). Axial highs are generally thought to result from buoyantly support provided by low-density, possibly partially molten material under the spreading center (Buck, 2001; Eberle et al., 1998). The generation of axial valleys at spreading centers is more controversial. The two earliest ideas about steady-state axial valleys relate either viscous flow or tectonic faulting. The viscous flow idea is that flow of viscous asthenosphere into a narrow slot between two lithospheric plates could produce a valley with flanking highs (Sleep, 1969). A difficulty with this model is that viscous stresses and related valley depth should scale with plate separation velocity; predicting the deepest valley for the fastest plates, contrary to what is seen.

The tectonic control of axial valley formation was proposed by Tapponier and Francheteau (1978) who suggested that the faulting of the brittle axial lithosphere should produce a valley. Offset of normal faults dipping toward the spreading axis should deepen a valley, but they did not specify what would limit the valley depth. Phipps Morgan et al. (1987) used simple mechanical arguments to suggest that the depth of a tectonically generated valley scales with the thickness of axial lithosphere.

Several observations and recent models do not fit the view that axial valley depth scales simply with axial lithospheric thickness. At spreading centers with very thick crust and no axial valley, like Iceland and Afar, seismicity extends to nearly 10 km depth at the spreading axis (Ayele et al., 2009; Einarsson and Brandsdottir, 1980). Such thick brittle lithosphere would support a deep valley according to the tectonic model. Numerical models that self-consistently treat the mechanics of faulting show that tectonic extension of lithosphere as thin as that inferred for fast spreading ridges should result in moderately deep axial valleys (Qin and Buck, 2005).

Gradual changes in axial valley depth along some slow spreading segments do not clearly correlate with changes in axial lithospheric thickness. For example, a seismic refraction study along the 33°S latitude segment on the Mid-Atlantic Ridge shows crustal thickness differences of a factor of two (Tolstoy et al., 1993) (Fig. 8). Most of the variation occurs in the seismically fast crustal layer 3, thought to be composed of gabbros. Layer 2 is thought to primarily consist of dikes formed in the cold, brittle crust. If this is correct then the uniform thickness of Layer 2 implies that axial lithospheric thickness is nearly constant along this segment. As shown in Fig. 1 there is almost no axial valley near the segment center while the valley relief is nearly 2 km at the segment end. It appears that the reduced magma supplies to the segment ends, not thicker lithosphere, results in a deeper valley there.

Chen and Morgan (1990) were the first to incorporate magmatic dike intrusion into a spreading center thermo-mechanical model. In their model, magma was injected as a dike opening at a rate equal to the spreading rate from the surface down to the base of the crust. They found that a valley only forms when the axial lithospheric thickness H_L is greater than the crustal thickness H_C. This is consistent with work suggesting that magma-filled dikes open at lower stress differences that needed for tectonic faulting (Rubin, 1992; Rubin and Pollard, 1988). The Chen and Morgan (1990) model lithospheric thickness and valley relief increase as spreading rate decreases, consistent with the observed trend. However, Poliakov and Buck (1998) found that the constant dike height model produces no faulting in a model that allows for strain localization. They also noted that this dike geometry resulted in a non-physical stress singularity at the base of the dike.

In a numerical model that assumes dikes open to the base of the axial lithosphere, Buck et al. (2005) reproduced the observed range of spreading center faulting. Their model fault pattern depends on the ratio M of the rate of dike widening to the rate of plate spreading. For M close to 0.5, large-offset faults develop on one side of the axis, similar to the detachment faults found along slow-spreading ridges (Cann et al., 1997; Cannat et al., 2006; Tucholke et al., 1998). For M between ~0.6 and 0.99 a series of nearly evenly spaced, moderate offset faults form in sequence, while for M between 0 and ~0.4 a more chaotic pattern of fairly large offset faults prevails (Olive et al., 2010; Tucholke et al., 2008). For $M = 1$ the model produces an axial high with a height that depends on the density structure at the axis compared to that off-axis. However, for all values of M less than 1 the axial valley depth is independent of M and equals the depth predicted for purely tectonic extension (Qin and Buck, 2005).

The Chen and Morgan (1990) and the Buck et al. (2005) models assume different dike heights, but depend on a similar ratio of the magma input flux to lithospheric spreading rate. If dikes supply all the magma to build the crust then $M = H_C/H_L$. However, one model does not produce faults and the other does not produce variations in axial valley relief with magma input. Ito and Behn (2008) tried to reconcile the 'M-based' approach with spreading rate dependent axial relief by assuming the near-axis region had a low effective viscosity that allowed the axis to rebound closer to local isostatic equilibrium. The viscosity of the axial lithosphere controls the axial relief while M still controls the faulting pattern. For the model to fit observations required that the effective viscosity depend on spreading rate. Though this works, it is not clear what this viscosity represents. In this paper we also try to reconcile observed variations in faulting and axial relief, but with a new approach.

3. Model formulation

We formulate a new treatment of dike opening that focuses on how dikes opening into the axial brittle–elastic lithosphere must also open some distance into the underlying ductile–viscous asthenosphere. A key is that during the short time that a dike opens and freezes elastic stresses generated in the asthenosphere change the distribution of dike opening in the lithosphere. Here the lithosphere is defined as the region that is strong enough to maintain significant elastic stresses over the long-time interval (i.e. 10–100 s of years) between dike events, while the asthenosphere can only maintain such stresses during an event. The lithosphere and the asthenosphere are assumed to be visco-elastic–plastic regions. The viscosity of the lithosphere is taken to be so high that negligible viscous relaxation of stresses occurs over any time scale of interest. In contrast, the asthenosphere is assumed to have such a low viscosity that it maintains zero elastic stresses on the time scale between dike intrusion events (10 s–100 s of years; e.g. Wright et al., 2012). For the purpose of the present analysis the dike event is taken to be instantaneous so that during the event the asthenosphere behaves elastically and can be strongly stressed.

We consider the opening of vertical, magma-filled dikes driven by extensional stresses produced by plate spreading at mid-ocean ridges. The analytic and numerical models developed here consider idealized cross-sections of a spreading center with the horizontal axis aligned in the plate spreading direction. The magma filling a dike is taken to come from lateral flow of magma along the spreading axis. Some justification for this is based on seismic and geodetic observations showing that magma chambers a few kilometers across at the centers of some spreading segments feed dikes that propagate as much as 70 km from those centers (Einarsson and Brandsdottir, 1980; Wright et al., 2012).

A critical feature of our new model is that the magma flux available to a part of a spreading center is split between lithosphere opening dikes, and deeply intruded gabbros. We first consider approximate analytic descriptions of the way axial depth should change the partitioning of magma between the elastic and viscous depth range at a spreading axis. Then we use our derived analytic relations between axial depth and lithospheric dike opening in the kind of two-dimensional, cross-sectional numerical models previously used to investigate faulting at ridges.

3.1. Parameterizing dike opening into the asthenosphere

The aim of the following analysis is to describe what controls the depth distribution of dike opening at a spreading center. Parameters defined are listed in Table 1. Because rocks have little resistance to tension, a dike can be assumed to open wherever magma pressure P_m is greater than the local minimum compressive stress (Delaney and McTigue, 1994; Rubin, 1995). For a vertical dike we define the driving pressure P_d as the difference between the magma pressure and horizontal stress σ_h as:

$$P_d = P_m - \sigma_h \tag{1}$$

We adopt the geologic convention that compressive stress is positive so that a dike should open where driving pressure is positive. For a mid-ocean ridge, the separation of plates should reduce the horizontal stress in the axial lithosphere and so promote the formation of vertical dikes. Comparably low stresses do not develop in the hot asthenosphere during slow extension between dike events due to thermally activated creep. However, the opening of a dike in a region of positive driving pressure, like axial lithosphere, will change the stresses in the surrounding region and can drive dike opening into an area of initially negative driving pressure, like the asthenosphere (Pollard, 1976; Weertman, 1971).

To estimate how far a dike could propagate into a region of negative driving pressure, Pollard (Pollard, 1976; Secor and Pollard, 1975) considered the simple case of linear variation of driving pressure with distance from the center of a dike opening in an elastic whole-space. By neglecting stress changes in the direction parallel to the dike plane and assuming zero fracture toughness, he was able to write an analytic expression for the distance of dike opening. For the case of positive driving pressure at the dike center, he found that the part of the dike opening in the region of negative driving pressure can be longer than the part in the region of positive driving pressures. Qin and Buck (2008) numerically treated dike opening for a half-space with a stress field expected for a mid-ocean ridge, where the positive driving stresses were initially confined to the lithosphere. Assuming zero fracture toughness they found a dike shape similar to that found by Pollard (1976), but the large magnitude of negative driving stress in their model asthenosphere gave them a smaller length of dike opening there compared to the analytic case.

A key point is that the change in axial depth does not change the lithostatic pressure in the fluid asthenosphere. If dikes open just to the top of the axial lithosphere, then increasing the axial valley depth D increases the magnitude of the negative driving pressures in the asthenosphere below a spreading axis. Here we derive a relation between the distance of dike opening, axial lithospheric stress and thickness and axial depth under the assumption that dikes, or a series of dikes, have their top at the depth of

Table 1
Summary of parameters.

Parameters	Description
D	Axial depth relative to local isostatic depth of near-axis region
H_c	Crustal thickness
H_L	Axial lithospheric thickness
V_p	Full spreading rate
P_d	Driving pressure
P_{dL}	Driving pressure in the lithosphere
P_m	Magma pressure
σ_h	Horizontal stress
z	Depth below the surface of near axis in isostatic equilibrium
z'	Depth below of the base of axial lithosphere
w_0	Dike width in lithosphere
$\Delta\rho_1$	Density difference between magma and crustal rock
$\Delta\rho_2$	Density difference between water and crustal rock
E_L	Energy released on dike opening in the lithosphere
E_A	Energy input required for dike opening in the asthenosphere
H_G	Distance of dike opening into asthenosphere
M	Lithospheric dike opening rate divided by V_p
ΔH_c, ω	Amplitude and period of oscillations in H_c
W_{ext}	Cross-axis extent of extrusion

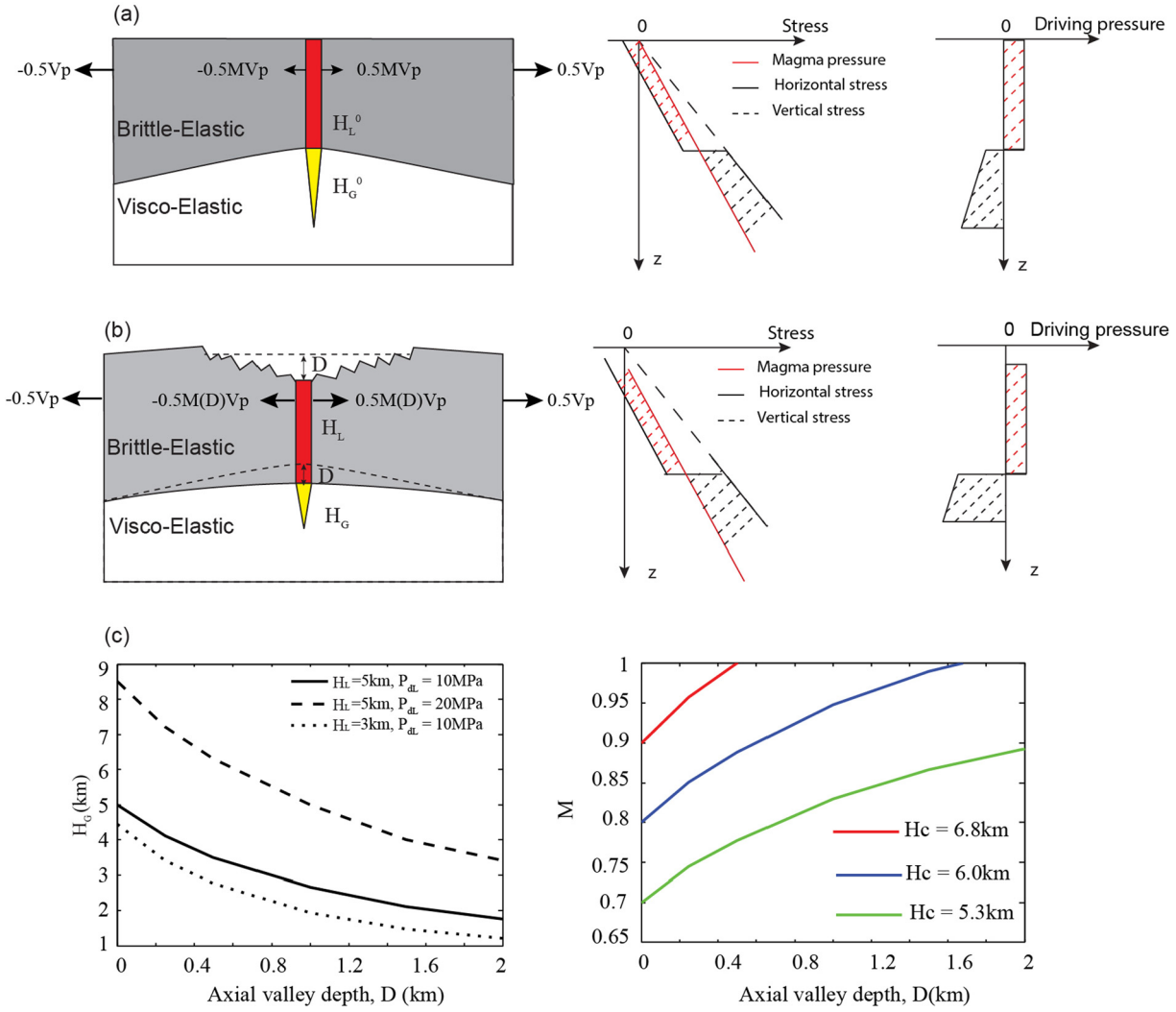

Fig. 2. Illustrations of the interaction between axial relief and magmatic dike intrusions. (a) Shows the distance H_G of dike sub-lithospheric opening into warmer asthenosphere where the axial depth D equals zero. The driving pressure in lithosphere P_{dL} is uniform, while the driving pressure in asthenosphere is negative and depends on axial lithospheric thickness H_L. The depth z is measured from the surface of the axial crust if it were in local isostatic equilibrium, the density difference between magma and country rock is $\Delta\ \rho_1$. (b) The formation of an axial valley with depth D lowers the pressure in magma at a given depth z and thus decreases the driving pressure in the asthenosphere. (c) Left panel shows the relation between H_G and axial valley depth for different values of axial lithospheric thickness and driving pressure. Right panel shows the relation between M and axial valley depth as defined in equations (12) and (14), the axial lithospheric thickness equals 5 km and the driving pressure is set to 10 MPa. The color of curves shows different crustal thickness Hc. (For interpretation of the colors in the figure(s), the reader is referred to the web version of this article.)

the spreading axis. Rather than do a full numerical treatment, we assume a simplified version of the dike geometry based on the numerical model of Qin and Buck (2008) and use energy arguments to estimate the distance of dike opening into the asthenosphere. We assume that the width, w, of a dike in lithosphere of thickness H_L is uniform and equal to w_0, while width of dike in asthenosphere decreases linearly with distance over a thickness H_G (Fig. 2(a)), so that:

$$w(z) = \begin{cases} w_0 & z' < 0 \\ w_0(1 - \frac{z'}{H_G}) & z' > 0 \end{cases} \tag{2}$$

where $z' = z - (H_L + D)$ is depth measured from the lithosphere–asthenosphere boundary, and $z = 0$ at the surface of the axial crust if it were in local isostatic equilibrium. Ideally, $z = 0$ should be set at the depth where accretion results in neither an axial valley nor an axial high. This reference depth has a simple definition only for the case of no lateral variations in lithospheric density structure outside a vanishingly narrow region of dike axial dike intrusion. This is one of the assumptions needed to derive an analytic description of axial relief (Buck, 2001). For more general axial lithospheric structures the value is close to the local isostatic depth of the axial region within about a flexural wavelength of the spreading axis. For simplicity, we define $z = 0$ as the local isostatic depth of the lithosphere at the side of our model domain. Taking $z = 0$ as the local isostatic depth of the near axis lithosphere would change our predicted axial relief by between 10 and 100 m.

The magma pressure is defined relative to the pressure at $z = 0$, and is assumed to be the static pressure in a column of magma with a top at the surface of the axial lithosphere so that:

$$P_m = \rho_w g D + \rho_m g (z - D) \tag{3}$$

where ρ_w is the density of water and ρ_m is the density of magma and g is the acceleration of gravity.

In the lithosphere the simplest assumption is that the driving pressure is uniform (Rubin, 1995; Rubin and Pollard, 1988). This means that the horizontal stress is a constant amount lower than the magma pressure. To first order, the width of the dike in the lithosphere is directly proportional to the driving pressure there. The fact that most dikes seen in the field are about a meter wide

is consistent with a set lithospheric driving pressure for each dike event (Qin and Buck, 2008).

In the asthenosphere, the horizontal stress should equal the lithostatic stress so that:

$$\sigma_h = \rho_c g z \quad z' > 0 \tag{4}$$

where ρ_c is the density of country rocks, assumed constant here. With these assumptions the driving pressure is negative in the asthenosphere and can be expressed as:

$$P_d = -\big((\rho_c - \rho_m)gz + (\rho_m - \rho_w)gD\big) \quad z' > 0 \tag{5}$$

Elastic strain energy is liberated as a dike opens and reduces extensional elastic stresses in the lithosphere. Taking the dike to be inviscid, the energy change equals the work done by the driving pressure on the wall of the dike as it opens. The driving pressure must equal zero when the dike is open to an equilibrium width $w(z)$ and we assume that the driving pressure drops linearly with width to zero as the dike opens. Then the energy change δE per unit length along the axis of dike opening is:

$$\delta E = \frac{1}{2} P_d w(z) \delta z \tag{6}$$

Because no work is done on the magma in the limit that its viscosity is vanishingly small, the elastic strain energy released as the dike opens in the lithosphere (E_L) should equal the energy consumed in forcing open the part of the dike in the asthenosphere (E_A) so:

$$E_L + E_A = 0 \tag{7}$$

The work done in the lithosphere given by integrating equation (6) is:

$$E_L = \frac{1}{2} P_{dL} w_0 H_L \tag{8}$$

where P_{dL} is the driving pressure in the lithosphere.

The energy consumed in the asthenosphere is:

$$E_A = \int_{H_L}^{H_G+H_L} \frac{1}{2} P_d(z) \cdot w(z) dz \tag{9}$$

Using equations (2), (5) and (9), we can rewrite E_A:

$$E_A = \frac{w_0}{2}\left[\frac{1}{2}(\Delta\rho_1 g H_L + \Delta\rho_2 g D) H_G + \frac{1}{6}\Delta\rho_1 g \cdot H_G^2\right] \tag{10}$$

where $\Delta\rho_1$ is the density difference between magma and crustal rock, and $\Delta\rho_2$ is the density difference between water and crustal rock. Setting the total energy change to zero gives:

$$H_L P_{dL} = \frac{1}{2}(\Delta\rho_1 g H_L + \Delta\rho_2 g D) H_G + \frac{1}{6}\Delta\rho_1 g \cdot H_G^2 \tag{11}$$

Solving the equation (11), we can express the H_G as:

$$H_G = \frac{-3\Delta\rho_1 g H_L - 3\Delta\rho_2 g D + \sqrt{9(\Delta\rho_1 g H_L + \Delta\rho_2 g D)^2 + 24\Delta\rho_1 g P_{dL} D H_L}}{2\Delta\rho_1 g} \tag{12}$$

Fig. 2(c) shows analytic results indicating that the deeper the axial valley, the shorter the downward distance of dike opening into the asthenosphere. The shorter this part of the dike, the smaller the amount of magma is driven into the asthenosphere to form gabbros.

We can now describe the flux of magma going into the asthenosphere as a function of D assuming the magma flux available to fill a dike on a part of a spreading center is equal to the oceanic crustal thickness H_C times the spreading rate V_P. Any decrease in flux going into the asthenosphere means that more can go into the part of the dike opening in the lithosphere. Given the simple geometry shown in Fig. 2(a) implies that:

$$H_C V_P = M V_P \left(H_L + \frac{1}{2} H_G\right) \tag{13}$$

MV_p is the dike opening rate in the lithosphere. Rearranging this equation allows us to describe the fractional opening rate of the lithospheric part of the dikes:

$$M = \frac{Hc}{H_L + \frac{1}{2} H_G(D)} \tag{14}$$

The relationship between M and D given by equation (14) is shown for several cases of lithospheric stress, thickness and crustal thickness in Fig. 2(c). Equation (14) is then used to specify the rate of lithospheric dike opening in the numerical models of axial stretching and faulting.

3.2. Numerical methods

To see how this analytic model affects valley formation and faulting patterns for a reasonable spreading center lithospheric structure and rheology, we used FLAC (Fast Lagrangian Analysis of Continua), an explicit hybrid finite-element and finite-difference technique, to solve the equations of conservation of mass and momentum in a visco-elastic–plastic continuum. This method has been used to simulate localized deformation in various tectonic settings and was described in detail elsewhere (Behn and Ito, 2008; Buck et al., 2005; Lavier et al., 2000; Poliakov and Buck, 1998).

We conducted two-dimensional numerical simulations of magmatic injection and fault growth for the same idealized and fixed ridge thermal structure considered by Buck et al. (2005). The material deforms according to a dry diabase flow law (Mackwell et al., 1998), which ensures that the region cooler than ~600 °C (lithosphere) behaves elasto-plastically, while the hotter areas behave visco-elastically. The brittle–ductile transition roughly coincides with the 600 °C isotherm for this flow law. A Mohr–Coulomb failure criterion is implemented in the lithosphere, assuming a friction coefficient of 0.6 and material cohesion of 25 MPa in intact material. Wherever this yield criterion is met, the material weakens with strain. To favor strain localization, 10 MPa of cohesion loss occurs over 1% of strain. Slower strain weakening (13 MPa of cohesion loss occurring over 30% of strain) continues after this initial phase of fast-strain weakening. Model elements near the ridge axis are 250 m wide, so the amount of fault slip necessary for total fault weakening is ~300 m (Lavier et al., 2000).

The dike opening rate in the numerical model is defined as M times Vp, with M described as a function of axial depth D given by equations (12) and (14) (Fig. 3). D is defined as the difference between the depth of the top axial element and the isostatic equilibrium level.

We assume that a series of dikes accommodates the separation of plates at a spreading axis with a uniform average opening rate with depth (i.e. M is uniform with depth in the lithosphere). Though the rate of dike opening in the asthenosphere should decrease with depth, we found some numerical difficulties in resolving fault patterns when we implemented depth dependent M. Since the rate of dike opening in the asthenosphere does not affect either the long-term axial relief or the faulting patterns (Behn and Ito, 2008; Poliakov and Buck, 1998), we assume the same rate

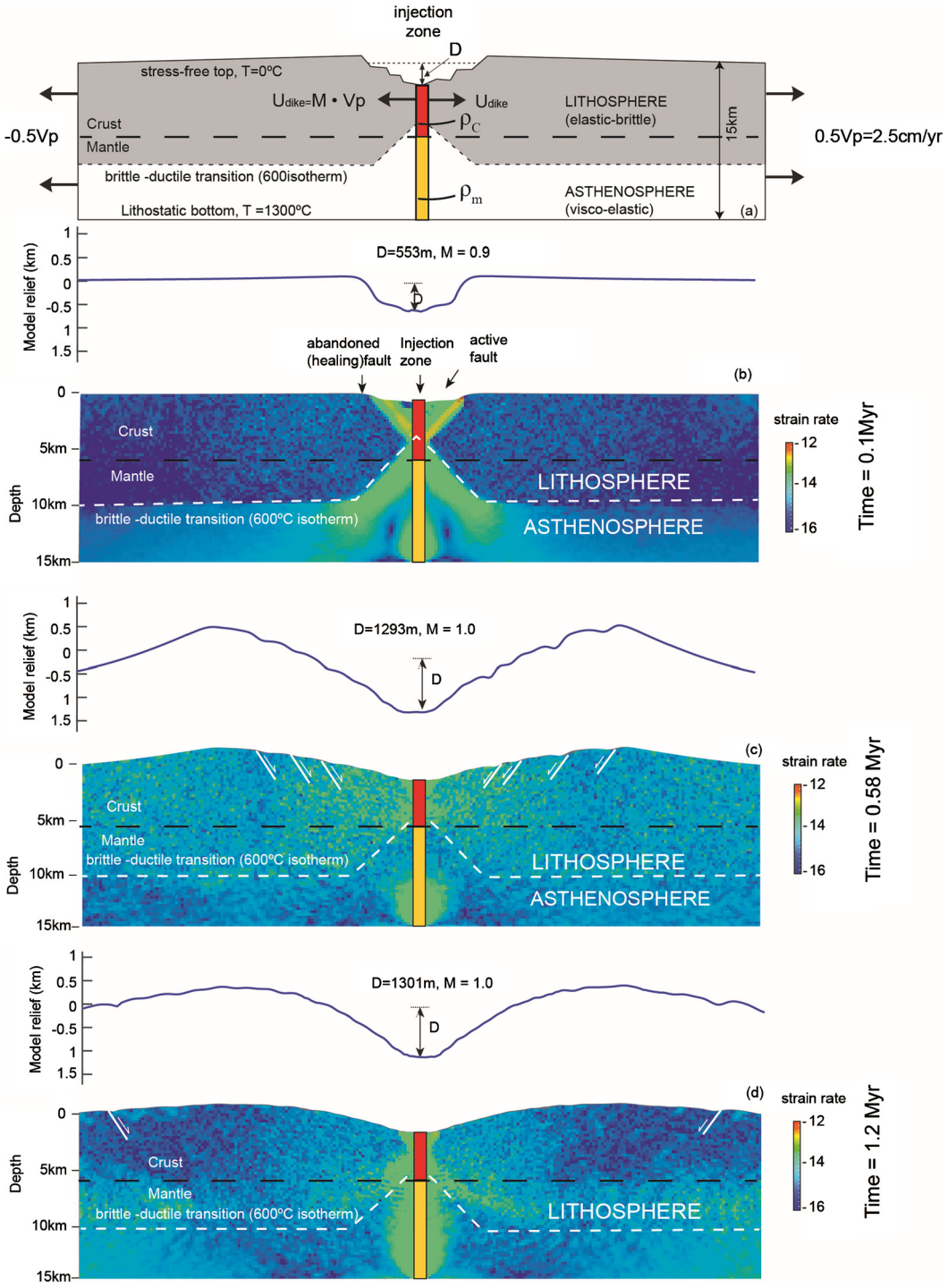

Fig. 3. Set up for numerical models with dikes that open into the axial lithosphere and ductile sub-lithospheric crust. (a) Set-up of the numerical model in which dikes open into both the axial lithosphere and the warm, ductile asthenosphere. (b)–(d), Snapshots of a simulation with $H_C = 6$ km, top panels are model topography and bottom panels are modeled distribution of strain rate. Fault scarps were identified as the steepest features that dip toward the axis.

of dike opening in the asthenosphere as in the lithosphere so that M is uniform over the whole height of the axial domain.

The domain is subjected to horizontal extension at a half-rate of 2.5 cm/yr, applied symmetrically on the side boundaries (Fig. 3). The top boundary has zero traction and the bottom is subject to lithostatic normal stress and no shear stress. Both are free to deform with the Lagrangian grid, which is periodically re-interpolated to a new grid with uniform horizontal grid spacing. On regridding, the bottom boundary is set to be horizontal and at each horizontal position the grid spacing is uniform between the free surface and the bottom boundary.

4. Numerical results

The numerical models illustrate that reasonable axial valley shapes result from our analytic estimate relating the fractional rate of dike opening in the axial lithosphere M to axial depth D. Our models show (Fig. 4) that the axial depth cannot increase without limit. Two mechanisms can stop axial deepening; one related

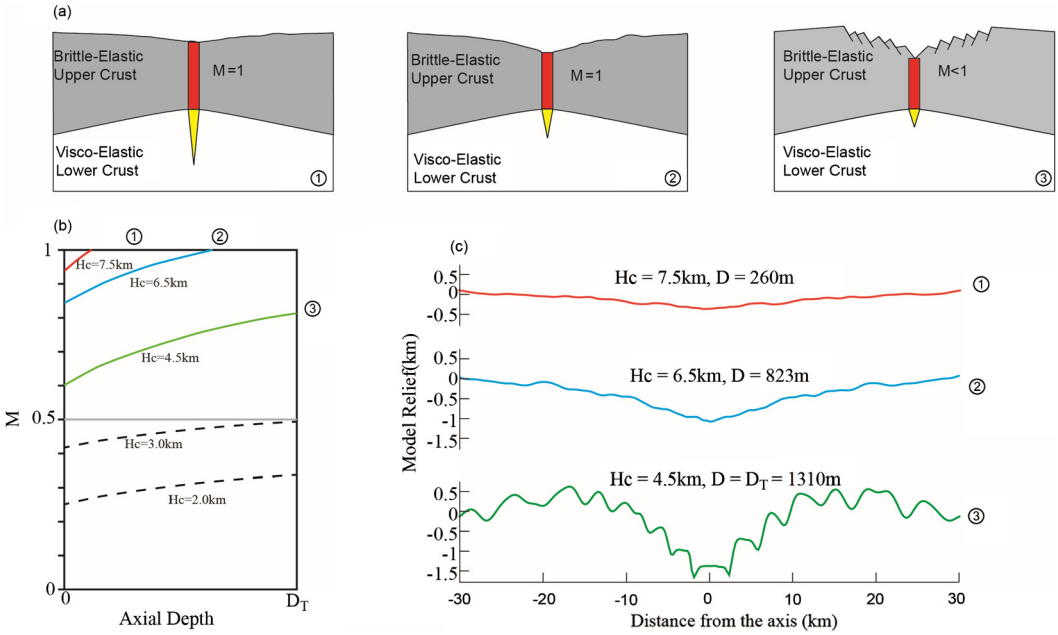

Fig. 4. Modeled axial relief and fault related relief when dikes open within and below the axial lithosphere. (a) Cartoons show conceptual relations between the depth distribution of dike opening, axial depths and fault relief for three values of the dike magma supply. (b) The relationship between axial depth and effective magmatic fraction M from equation (14) for different crustal thickness. (c) Numerically model bathymetry profiles for cases in which crustal thickness H_C varied as shown. The cases illustrated with red and blue solid lines do not show clear faulting but have different axial depths; the case shown in green shows fault-related relief.

to magma input and the other to tectonics. If $M < 1$ the dikes do not open as fast as the plates spread. Thus, faults form and the offset of those faults cause an axial valley to deepen. In the magma-controlled mode axial depth will stop increasing when the model 'self-adjusts' so that M equals 1: As the valley depth D increases the value of M increases as indicated by Equation (14). When M equals 1 the valley stops deepening. In contrast, tectonics takes over if the axial depth reaches the maximum tectonically controlled axial valley depth D_T and M is still less than 1. In that case the axial depth will remain at D_T, as it is maintained by continual faulting. As noted by Qin and Buck (2005), D_T is controlled by axial lithospheric thickness and the rate of off-axis lithospheric thickening (i.e., slope of the lithosphere–asthenosphere boundary). The fault patterns in the tectonic controlled mode depend on magma input, but the valley depth does not. Results for fault patterns are consistent with previous M-based models (Behn and Ito, 2008; Buck et al., 2005; Ito and Behn, 2008; Olive et al., 2015; Tucholke et al., 2008).

A minor problem with our model is that it predicts no faulting for cases with magmatic control of the axial valley depth. However, observations suggest that even ridges with shallow valleys have small normal faults that are relatively continuous along strike (see Fig. 1). There are several ways that these faults might be produced and we briefly consider a mechanism driven by minor oscillations in the amount of magma delivered to dikes.

In the magma-controlled mode magmatic oscillations should lead to extrusion sometime and faulting at other times (see Fig. 5). To treat magmatic fluctuations, we set:

$$H_C(t) = H_C(0) + \Delta H_C \sin(2\pi\omega t) \tag{15}$$

where ΔH_C and ω are the amplitude and period of magma supply oscillations. We incorporate this relation into equation (14) to compute temporal variations in M. Since values of M greater than 1 are non-physical, we set $M = 1$ when $H_c > H_L + \frac{1}{2}H_G(D)$. In that case we also emplace new extrusive material above the location of the dike at a rate equal $(H_c(t) - H_L - \frac{1}{2}H_G(D))V_p/W_{ext}$, in which W_{ext} is the cross-axis extent of extrusion. The numerical results (Fig. 6) show that the faults patterns are directly related to magmatic fluctuation amplitude ΔH_C. For a given period, topographic roughness increase with larger ΔH_c (Fig. 6). The detailed influence of magmatic oscillations on faulting patterns is, however, complex. For periods ω greater than the time interval between successive faults (represented by the average fault spacing), fault spacing is controlled by the temporal variability between tectonic and magmatic periods (Fig. 6); for shorter magmatic fluctuation periods, fault spacing become independent of ω for a given magmatic fluctuation amplitude, as was describe by Ito and Behn (2008) and Olive et al. (2015).

5. Discussion

This analysis shows that adding parameterized effects of discrete diking events to a model that already fit the range of faulting seen at spreading centers allows it to reproduce the observed range of axial relief. Before comparing model predictions with observations we discuss how axial valleys can be maintained when dikes accommodate all plate spreading without significant faulting.

5.1. How the model works

The key to this model is that the opening of a dike in the lithosphere generates elastic stresses in the asthenosphere that forces opening of a dike some distance into the asthenosphere. The amount of dike opening in the asthenosphere depends on the depth of the axis, such that the deeper the axis the less magma goes in to the part of the dike opening in the asthenosphere (i.e. H_G depends on D). If there is not enough magma available to open the dike in both the lithosphere and the asthenosphere when $D = 0$ then fault offset deepens the valley. Eventually, for a given valley depth, there may be enough magma for the dikes to open at the full spreading rate (i.e. $M = 1$). As viscoelastic stresses relax after a diking event the magma in the asthenospheric part of the dike should rise to the base of the lithosphere and cool to form gabbro. For cases where the lithosphere is thinner than the crust this material is added directly to the crustal thickness. For cases

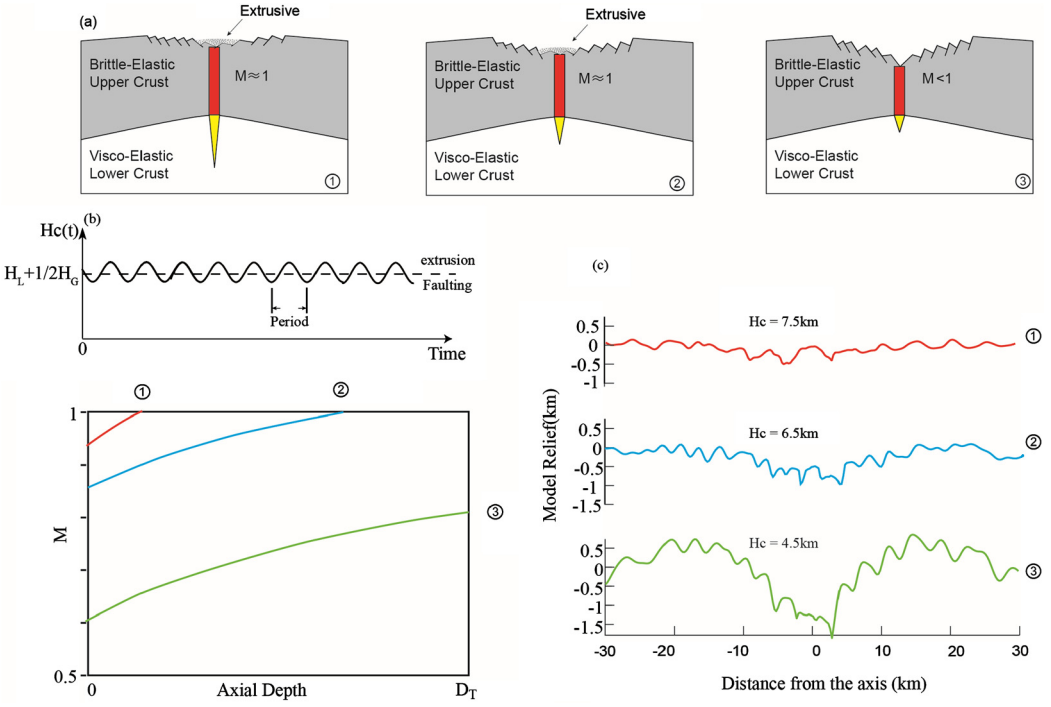

Fig. 5. Modeled faulting and axial relief for cases with magma supply fluctuation. (a) Cartoon illustrating how fluctuation in magma supply can produce faults for any value of the average magma supply. (b) Upper panel shows Hc evolution with time. When $H_C > H_L + 1/2H_G$, extrusion will occur, when $H_C < H_L + 1/2H_G$, faults will develop. Lower panel show the analytic relationships between axial depth and M for these cases. (c) Numerical model bathymetry profiles for cases in which tectono-magmatic period, $\omega = 0.1$ Myr, amplitude of magmatic oscillation, $\Delta H_C = 0.1$ and $H_C(0)$ as shown.

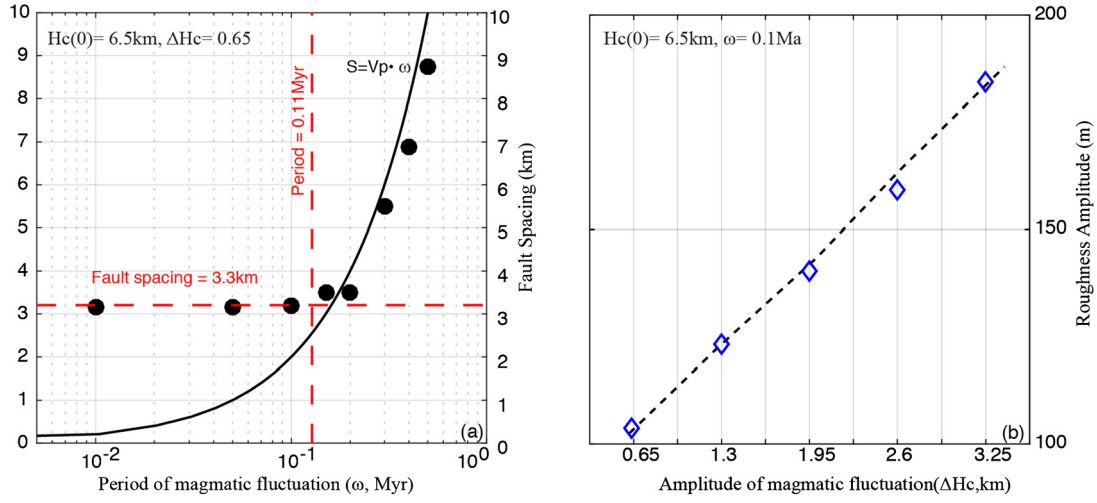

Fig. 6. Sensitivity of model fault pattern to magmatic supply fluctuation period and amplitude for model with half spreading rate equals to 2.5 cm/yr and axial lithospheric thickness is set to be 5 km. (a) Results of cases with $H_C(0) = 6.5$ km, $\Delta H_C = 0.65$. Black circles show spacing of modeled faults, measured by the distance between the tops of the faults, versus period of magmatic fluctuations, black solid line shows a linear relation between spacing and period. (b) Results of cases with $H_C(0)$ fixed at 6.5 km, ω fixed at 0.1 Myr. Blue diamonds show roughness amplitude (roughness is the average of the absolute difference between each point in the filtered profile and the median value of the profile) of modeled faults versus amplitude of magmatic fluctuations.

where the lithosphere is thicker, the added material may produce isolated gabbro bodies in the lithosphere.

This model only works if the viscosity of the asthenosphere is in a range allowing stresses to relax between dike events while maintaining stresses during events. This is tenable if the asthenospheric Maxwell Time (τ_M = viscosity/shear modulus) is more than a few days and less than a few years, implying a viscosity between $\sim 10^{15}$ and 10^{20} Pa s. Geodetic measurements for the viscoelastic deformation around the active dike intrusion in the Afar of Ethiopia gives an asthenospheric viscosity of a few times 10^{18} Pa s (Nooner et al., 2009), which is in the required range.

Model results also depend on the assumed value of the driving stress to open dikes in the lithosphere P_{dL}. The preponderance of $\sim$1 m wide dikes seen in ophiolites, the exposed sections of fossil spreading centers, argues for driving pressure on the order of 10 MPa (Qin and Buck, 2008). If the driving pressure is vanishingly small, the model will give the same unsatisfying result in terms of axial relief as previous models with constant M for spreading centers (Buck et al., 2005; Ito and Behn, 2008; Olive et al., 2015; Tucholke et al., 2008). This can be seen by setting P_{dL} equal to 0 in equations (12) and (14) which makes M independent of axial depth D and equal to Hc/H_L.

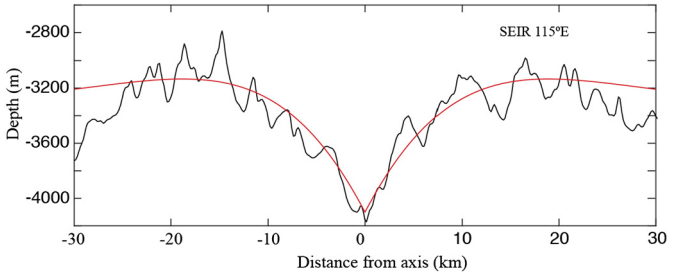

Fig. 7. Illustration of the way flexture of a plate accreted below the level of local isostatic equilibrium can produce a axial valley. Comparison of observed profile from Southeast Indian Ridge (black) and analytic axial relief from flexural accretional model (red) derived in Buck (2001) (for flexure parameter equal to 12 km and axial depth D set to −800 m).

In the newly defined magmatic mode, axial valleys are maintained when magmatic dike opening accommodates all lithospheric plate separation. This may seem surprising since valleys are typically associated with lithosphere-cutting normal faults that do not occur in this mode. Though the numerical models show that valleys can be maintained without such faulting, they do not show how this occurs. As noted above, the combination of finite sized diking events (i.e. with a finite value of P_{dL}) and a finite supply of magma per event can result in accretion of dikes with a top at a depth D that is lower than the reference level where $z = 0$. Those dikes freeze onto the side of the lithospheric plates before the elastic stresses in the asthenosphere relax. If the dike were not attached to these plates, the new dike would rise to be in local equilibrium (i.e. where $D = 0$) as those asthenosphere stresses relax. Being attached to the lithosphere, the upward push of the newly accreted dike causes distributed flexure of the lithosphere. It is the flexural strength of the plate that maintains the valley.

This is precisely the same mechanism of accretional flexure, or accretional curvature, previously suggested to explain axial highs (Buck, 2001). The difference is that for axial highs the dikes accrete above their level of local isostasy while for axial valleys, dike accretes below this level. With a change in sign and amplitude the analytic axial relief derived in Buck (2001) is very similar to valleys seen in the magma controlled numerical models and in nature as shown in Fig. 7.

This flexural analysis is at the heart of the explanation of the tectonic control of the maximum valley depth. As the valley deepens the flexural stresses and so the bending moment maintained on the flanks of the axis increase. Lithosphere with finite strength can only support moments less than a maximum value (Turcotte and Schubert, 2014). The maximum depth of the axis, D_T, is the depth that makes the moment equal the maximum supportable moment, as described by Qin and Buck (2005).

5.2. Comparison of model predictions and observations

The model of magma partitioning between dikes in the lithosphere and gabbro below the lithosphere explains a range of observations not consistent with previously accepted models for axial valley formation (Chen and Morgan, 1990; Phipps Morgan and Chen, 1993). Unlike those models, the new approach implies that valleys can form in places where the axial lithosphere is thinner than the crust. This prediction is consistent with observations of the seismicity and seismic structure of several ridges with axial valleys. For example, at the TAG segment of the Mid-Atlantic Ridge, the maximum depth of seismicity, thought to mark the base of brittle lithosphere (deMartin et al., 2007), is less than the depth to the seismically imaged Moho (Canales et al., 2007; Zhao et al., 2012). Recent studies showed the crustal thickness near 58°28′E on the Southwest Indian Ridge is up to 9.5 km and this is much larger than axial lithosphere thickness as measured by the depth of axial magma chamber (Jian et al., 2017).

If the axial valley is at its maximum depth D_T, then the mode of faulting depends directly on the value of M, as detailed in previous models and consistent with observations (Behn and Ito, 2008; Cannat et al., 2006; Ito and Behn, 2008). In contrast, shallower steady-state axial valleys can be maintained with no faults. Small faults may form in response to oscillation in the magma supply, and characteristic fault offsets depend on the amplitude and period of these oscillations (Fig. 6). Such oscillations should also produce periodic extrusions. Available evidence suggests that eruptive volume produced during single eruptive episodes increase with decreasing spreading rate (Curewitz and Karson, 1998; Perfit and Chadwick, 1998; Rubin et al., 2009; Sinton et al., 2002). If this is so, then we would expect that the amplitude of magma supply variations, quantified using equations (14) and (15), would be inversely related to spreading rate. Then our model would be consistent with the observed trend of increasing fault offset with decreasing spreading rate. The magma supply oscillation may be induced by internal ridges processes and/or by external processes, such as climate-induce sea-level changes (Crowley et al., 2015).

Along many slow-spreading segments, axial relief and average fault offset increase with the distance from the segment center (Shaw and Lin, 1993). This is clear near 33°S on the mid-Atlantic ridge, which is one of only places where seismic refraction constraints on crustal structure are available along an entire segment (Fig. 8). The prediction that the amount of dike-supplied gabbros decreases with increasing axial depth is consistent with the seismic interpretation that the sub-dike layer 3 thins with distance from the segment center. As shown in Fig. 8, our model can explain the trend in axial relief if crustal thickness H_C decreases with distance from the segment center. Though we do not yet have a clear view of why such magma supply variation occurs, we hope that further work on magma-tectonic interactions will shed light on underlying segment-scale processes.

To relate model predictions with the global trends of axial relief as functions of lithospheric and crustal thickness, we can focus on the predicted conditions for the magma controlled mode of axial relief. We can get a closed form solution for D as function of H_L and H_C for that mode by combining equations (12) into (14), and setting $M = 1$. The results of doing this are plotted in shaded region of Fig. 9.

For the region in the upper left corner of Fig. 9, we expect that there will be axial highs with heights depending on the local buoyancy. Buoyancy refers to axial density structure (Buck, 2001; Buck et al., 2005). Fast spreading ridges like the East Pacific Rise and some intermediate spreading rate ridges like Juan de Fuca Ridges should belong to this region. The lower right corner in Fig. 9 shows the region of tectonic control on axial valley depth. The tectonic limit on axial valley depth D_T is expected to be a function of both axial lithospheric thickness H_L, and the geometry of lithospheric structure (Qin and Buck, 2005).

The essential new feature of our model is that we define a region between buoyancy and tectonic control of axial relief (shaded region in Fig. 9). In this transition region, it is the relation between magmatism and axial depth that controls the axial relief. The exact position of the boundaries depends on uncertain assumptions. For example, lowering the density contrast between magma and lower crust moves the region of magmatic control of axial valley depth to lower values of H_L. Assuming that a smaller fraction of the magma delivered to the crust is available to feed dikes moves this region to higher values of H_C. Even with these uncertainties

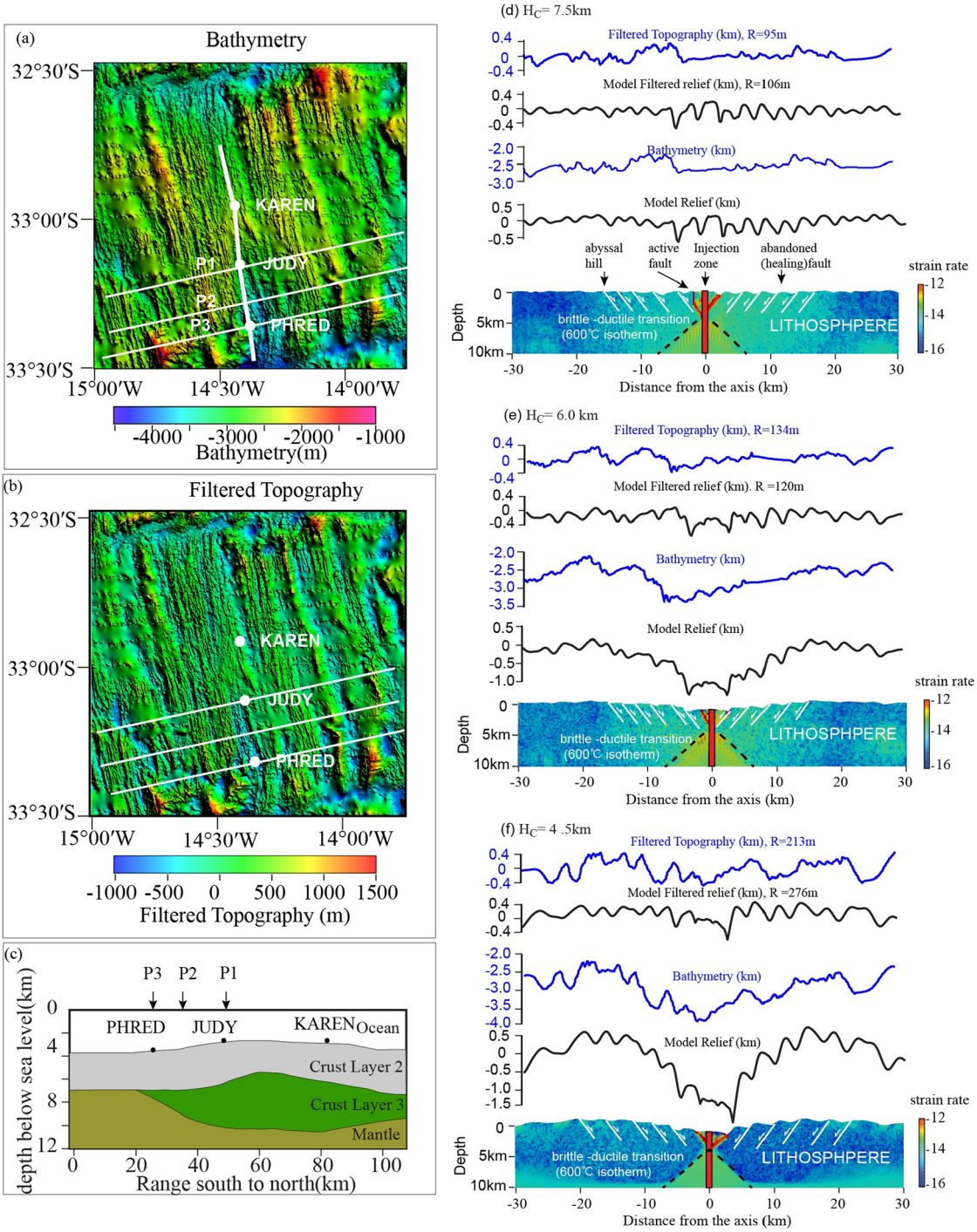

Fig. 8. Comparison of data and numerical model results for segment-scale variations in axial relief and faulting (a) Shaded relief bathymetric map of 33°S on the mid-Atlantic Ridge, Karen, Judy and Phred are location of OBSs from Tolstoy et al. (1993) (b) high-pass filtered bathymetry with wavelengths greater than 20 km removed. Filtered topography is expected to indicate fault characteristics (Small, 1998); (c) Along-axis interpreted cross-section of the 33°S segment of the Mid-Atlantic Ridge based on a seismic refraction experiment (Tolstoy et al. (1993)). (d)–(f) Three model cases for different values of axial crustal thickness Hc, but with the same lithospheric structure (axial lithospheric thickness HL is fixed at 5 km) and magma supply fluctuation period (0.1 Ma). Hc is based on seismic refraction experiment (Fig. 8(c)). (d) Note the fairly shallow axial valley and the moderate fault offsets for $Hc = 7.5$ km, which matches the sense of the bathymetric profile from 33°S Mid-Atlantic Ridge segment center (from Fig. 8(a), P1). (e) Deeper valley depth for $Hc = 6$ km. The model topographic profile is similar to that observed from Fig. 8(a), P2. (f) Faults with very large offsets occur and much deeper valley depth is seen for $Hc = 4.5$ km. The model topographic profile is similar to that observed from the 33°S segment end (Fig. 8(a), P3).

we are confident of the general patterns of axial relief as functions of H_L and H_C as show in Fig. 9.

6. Conclusions

Our treatment of partitioning of magma between lithosphere cutting dikes and deeper dikes resolves several problems of previous models for the accretion and tectonics of plate spreading centers. In summary, this conceptually simple mechanism implies that:

1. The global and segment-scale dependence of axial valley depth on crustal thickness and axial lithospheric thickness can be described analytically with the assumption that the amount

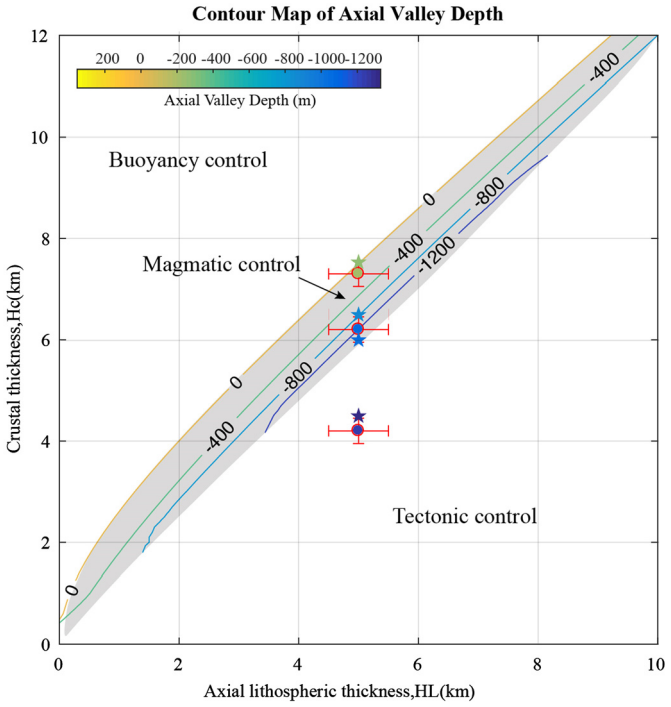

Fig. 9. The colored curves in the shaded region show the prediction of axial valley depth D for the model of axial relief controlled by magma input. Plugging equation (12) into (14), and setting $M = 1$, we get a prediction of D as a function of crustal thickness H_C and axial lithospheric thickness H_L. The average driving pressure in the lithosphere P_{dL} is assumed equals 10 MPa, the density difference between magma and crustal rock $\Delta\rho_1$ is 300 kg/m^3, and the density difference between magma and crustal rock $\Delta\rho_2$ is 2000 kg/m^3. For the region to the left and above the shaded region we expect axial highs with heights depending on the local buoyancy that is not treated here. The lower right region shows the parameter range of tectonic control on axial valley depth that should depend on axial lithospheric structure not treated fully here. Data on axial relief from Fig. 1(b) (circles) is displayed using the same color scale. The crustal thickness of data from Fig. 1(b) is constrained by seismic data (Tolstoy et al., 1993) and the axial lithospheric thickness is assumed to uniform and equal to 5 km. Four numerical prediction of axial valley (stars) is superimposed in the map using the same color scale.

of magma available to feed dike opening scales with local crustal thickness.

2. Axial valleys can be maintained without faulting when all plate spreading is accommodated by dike intrusion (i.e. where $M = 1$).

3. Oscillations in the magma supply may produce the observed faulting at ridges where axial depth shallower than maximum tectonic control depth D_T.

4. Large fault offsets occur when the axial valley is at the tectonically controlled maximum depth. The fault offset in the tectonic controlled mode depends on M as predicted by previous models.

This study allowed us to relate axial lithospheric and crustal thickness to the mechanics of dike opening and the related magmatic control of axial relief. Magma input should affect the thermal structure and thickness of the lithosphere. Thus, in future work we plan to show how combining thermal and mechanical models will allow estimation of the dependence of axial relief on spreading rate and crustal thickness for all three of the modes of axial relief.

Acknowledgements

Discussions with and comments from Jean-Arthur Olive, Jianghai Li, Guting Hou, Xiaochuan Tian and Yen-Joe Tan greatly improved the manuscript, as did excellent reviews by Garrett Ito and Richard Katz. Supported by National Science Foundation [Awards OCE-1658072 and OCE-1654745]. Z.L. appreciates the China Scholarship Council (CSC) 201606010067 for supporting a joint PhD student Project.

References

Ayele, A., Keir, D., Ebinger, C., Wright, T.J., Stuart, G.W., Buck, W.R., Jacques, E., Ogubazghi, G., Sholan, J., 2009. September 2005 mega-dike emplacement in the Manda-Harraro nascent oceanic rift (Afar depression). Geophys. Res. Lett. 36.

Behn, M.D., Ito, G., 2008. Magmatic and tectonic extension at mid-ocean ridges: 1. Controls on fault characteristics. Geochem. Geophys. Geosyst. 9.

Buck, W., 2001. Accretional curvature of lithosphere at magmatic spreading centers and the flexural support of axial highs. J. Geophys. Res., Solid Earth 106, 3953–3960.

Buck, W.R., Lavier, L.L., Poliakov, A.N., 2005. Modes of faulting at mid-ocean ridges. Nature 434, 719–723.

Canales, J.P., Sohn, R.A., Demartin, B.J., 2007. Crustal structure of the Trans-Atlantic Geotraverse (TAG) segment (Mid-Atlantic Ridge, 26° 10′N): implications for the nature of hydrothermal circulation and detachment faulting at slow spreading ridges. Geochem. Geophys. Geosyst. 8.

Cann, J., Blackman, D., Smith, D., McAllister, E., Janssen, B., Mello, S., Avgerinos, E., Pascoe, A., Escartin, J., 1997. Corrugated slip surfaces formed at ridge-transform intersections on the Mid-Atlantic Ridge. Nature 385, 329.

Cannat, M., Sauter, D., Mendel, V., Ruellan, E., Okino, K., Escartin, J., Combier, V., Baala, M., 2006. Modes of seafloor generation at a melt-poor ultraslow-spreading ridge. Geology 34, 605–608.

Carbotte, S.M., Macdonald, K.C., 1994. Comparison of seafloor tectonic fabric at intermediate, fast, and super fast spreading ridges: influence of spreading rate, plate motions, and ridge segmentation on fault patterns. J. Geophys. Res., Solid Earth 99, 13609–13631.

Chen, Y., Morgan, W.J., 1990. A nonlinear rheology model for mid-ocean ridge axis topography. J. Geophys. Res., Solid Earth 95, 17583–17604.

Crowley, J.W., Katz, R.F., Huybers, P., Langmuir, C.H., Park, S.-H., 2015. Glacial cycles drive variations in the production of oceanic crust. Science 347, 1237–1240.

Curewitz, D., Karson, J.A., 1998. Geological consequences of dike intrusion at mid-ocean ridge spreading centers. In: Faulting and Magmatism at Mid-Ocean Ridges, pp. 117–136.

Delaney, P., McTigue, D., 1994. Volume of magma accumulation or withdrawal estimated from surface uplift or subsidence, with application to the 1960 collapse of Kilauea Volcano. Bull. Volcanol. 56, 417–424.

deMartin, B.J., Sohn, R.A., Canales, J.P., Humphris, S.E., 2007. Kinematics and geometry of active detachment faulting beneath the Trans-Atlantic Geotraverse (TAG) hydrothermal field on the Mid-Atlantic Ridge. Geology 35, 711–714.

Eberle, M.A., Forsyth, D.W., Parmentier, E.M., 1998. Constraints on a buoyant model for the formation of the axial topographic high on the East Pacific Rise. J. Geophys. Res. 1031, 12291–12308.

Einarsson, P., Brandsdottir, B., 1980. Seismological Evidence for Lateral Magma Intrusion During the July 1978 Deflation of the Krafla Volcano in NE-Iceland. Raunvísindastofnun Háskólans.

Ito, G., Behn, M.D., 2008. Magmatic and tectonic extension at mid-ocean ridges: 2. Origin of axial morphology. Geochem. Geophys. Geosyst. 9.

Jian, H., Singh, S.C., Chen, Y.J., Li, J., 2017. Evidence of an axial magma chamber beneath the ultraslow-spreading Southwest Indian Ridge. Geology 45, 143–146.

Lavier, L.L., Buck, W.R., Poliakov, A.N., 2000. Factors controlling normal fault offset in an ideal brittle layer. J. Geophys. Res. 105, 431–442.

Macdonald, K.C., 1982. Mid-ocean ridges: fine scale tectonic, volcanic and hydrothermal processes within the plate boundary zone. Annu. Rev. Earth Planet. Sci. 10, 155–190.

Mackwell, S., Zimmerman, M., Kohlstedt, D., 1998. High-temperature deformation of dry diabase with application to tectonics on Venus. J. Geophys. Res., Solid Earth 103, 975–984.

Nooner, S.L., Laura, B., Eric, C., Roger, B.W., Hamling, I.J., Wright, T.J., Elias, L., 2009. Post-rifting relaxation in the Afar region, Ethiopia. Geophys. Res. Lett. 36, 147–148.

Olive, J.-A., Behn, M.D., Ito, G., Buck, W.R., Escartín, J., Howell, S., 2015. Sensitivity of seafloor bathymetry to climate-driven fluctuations in mid-ocean ridge magma supply. Science 350, 310–313.

Olive, J.-A., Behn, M.D., Tucholke, B.E., 2010. The structure of oceanic core complexes controlled by the depth distribution of magma emplacement. Nat. Geosci. 3, 491–495.

Perfit, M.R., Chadwick, W.W., 1998. Magmatism at mid-ocean ridges: constraints from volcanological and geochemical investigations. In: Faulting and Magmatism at Mid-Ocean Ridges, pp. 59–115.

Phipps Morgan, J., Chen, Y., 1993. Dependence of ridge-axis morphology on magma supply and spreading rate. Nature 364, 706–708.

Phipps Morgan, J., Parmentier, E., Lin, J., 1987. Mechanisms for the origin of mid-ocean ridge axial topography: implications for the thermal and mechanical structure of accreting plate boundaries. J. Geophys. Res., Solid Earth 92, 12823–12836.

Poliakov, A.N., Buck, W.R., 1998. Mechanics of stretching elastic–plastic–viscous layers: applications to slow-spreading mid-ocean ridges. In: Faulting and Magmatism at Mid-Ocean Ridges, pp. 305–323.
Pollard, D.D., 1976. On the form and stability of open hydraulic fractures in the Earth's crust. Geophys. Res. Lett. 3, 513–516.
Qin, R., Buck, W.R., 2005. Effect of lithospheric geometry on rift valley relief. J. Geophys. Res., Solid Earth 110.
Qin, R., Buck, W.R., 2008. Why meter-wide dikes at oceanic spreading centers? Earth Planet. Sci. Lett. 265, 466–474.
Rubin, A.M., 1992. Dike-induced faulting and graben subsidence in volcanic rift zones. J. Geophys. Res., Solid Earth 97, 1839–1858.
Rubin, A.M., 1995. Propagation of magma-filled cracks. Annu. Rev. Earth Planet. Sci. 23, 287–336.
Rubin, A.M., Pollard, D.D., 1988. Dike-induced faulting in rift zones of Iceland and Afar. Geology 16, 413–417.
Rubin, K.H., Sinton, J.M., Maclennan, J., Hellebrand, E., 2009. Magmatic filtering of mantle compositions at mid-ocean-ridge volcanoes. Nat. Geosci. 2, 321–328.
Secor, D.T., Pollard, D.D., 1975. On the stability of open hydraulic fractures in the Earth's crust. Geophys. Res. Lett. 2, 510–513.
Shaw, P.R., Lin, J., 1993. Causes and consequences of variations in faulting style at the Mid-Atlantic Ridge. J. Geophys. Res., Solid Earth 98, 21839–21851.
Sinton, J., Bergmanis, E., Rubin, K., Batiza, R., Gregg, T.K., Grönvold, K., Macdonald, K.C., White, S.M., 2002. Volcanic eruptions on mid-ocean ridges: new evidence from the superfast spreading East Pacific Rise, 17–19 S. J. Geophys. Res., Solid Earth 107.
Sleep, N.H., 1969. Sensitivity of heat flow and gravity to the mechanism of sea-floor spreading. J. Geophys. Res. 74, 542–549.
Small, C., 1998. Global systematics of mid-ocean ridge morphology. In: Faulting and Magmatism at Mid-Ocean Ridges, pp. 1–25.
Tapponnier, P., Francheteau, J., 1978. Necking of the lithosphere and the mechanics of slowly accreting plate boundaries. J. Geophys. Res., Solid Earth 83, 3955–3970.
Tolstoy, M., Harding, A.J., Orcutt, J.A., 1993. Crustal thickness on the Mid-Atlantic Ridge: Bull's-eye gravity anomalies and focused accretion. Science 262, 726–729.
Tucholke, B.E., Behn, M.D., Buck, W.R., Lin, J., 2008. Role of melt supply in oceanic detachment faulting and formation of megamullions. Geology 36, 455–458.
Tucholke, B.E., Lin, J., Kleinrock, M.C., 1998. Megamullions and mullion structure defining oceanic metamorphic core complexes on the Mid-Atlantic Ridge. J. Geophys. Res., Solid Earth 103, 9857–9866.
Turcotte, D.L., Schubert, G., 2014. Geodynamics. Cambridge University Press.
Weertman, J., 1971. Theory of water-filled crevasses in glaciers applied to vertical magma transport beneath oceanic ridges. J. Geophys. Res. 76, 1171–1183.
Wright, T.J., Sigmundsson, F., Pagli, C., Belachew, M., Hamling, I.J., Brandsdóttir, B., Keir, D., Pedersen, R., Ayele, A., Ebinger, C., 2012. Geophysical constraints on the dynamics of spreading centres from rifting episodes on land. Nat. Geosci. 5, 242–250.
Zhao, M., Canales, J.P., Sohn, R.A., 2012. Three-dimensional seismic structure of a Mid-Atlantic Ridge segment characterized by active detachment faulting (Trans-Atlantic Geotraverse, 25°55′N–26°20′N). Geochem. Geophys. Geosyst. 13.